Selective catalytic reduction of NO over Fe-ZSM-5: Mechanistic insights by operando HERFD-XANES and valence-to-core XES spectroscopy

Alexey Boubnov[†,§], Hudson W. P. Carvalho[†], Dmitry E. Doronkin[†,§], Tobias Günter[†], Erik Gallo[‡], Andrew J. Atkins[ξ], Christoph R. Jacob[ξ,*], Jan-Dierk Grunwaldt[†,§,*]

[†]Institute for Chemical Technology and Polymer Chemistry, Karlsruhe Institute of Technology, Engesserstr. 20, D-76131 Karlsruhe, Germany

[§]Institute for Catalysis Research and Technology, Karlsruhe Institute of Technology, Hermann-von-Helmholtz-Platz 1, D-76344 Eggenstein-Leopoldshafen, Germany

[‡]European Synchrotron Radiation Facility, 6 rue Jules Horowitz, BP 220, F-38043 Grenoble Cedex, France

[ξ]Center for Functional Nanostructures and Institute of Physical Chemistry, Karlsruhe Institute of Technology, Wolfgang-Gaede-Str. 1a, D-76131 Karlsruhe, Germany

ABSTRACT: An in-depth understanding of the active site requires advanced *operando* techniques and the preparation of defined catalysts. We elucidate here the mechanism of the selective catalytic reduction of NO by NH_3 (NH_3-SCR) over a Fe-ZSM-5 zeolite catalyst. 1.3 wt% Fe-ZSM-5 with low nuclearity Fe sites was synthesized, tested in the SCR reaction and characterized by UV-Vis, X-ray absorption near edge structure (XANES), and extended X-ray absorption fine structure (EXAFS) spectroscopy. Next, this defined Fe-zeolite catalyst was studied by complementary high-energy-resolution fluorescence-detected XANES (HERFD-XANES) and valence-to-core X-ray emission spectroscopy (V2C XES) under different model *in situ* and realistic working (*operando)* conditions identical to the catalyst test bench including the presence of water vapor. HERFD-XANES uncovered that the coordination (between 4 and 5), geometry (tetrahedral, partly 5-fold), and oxidation state of the Fe centres (reduced in NH_3, partly in SCR mixture, slight reduction in NO) strongly changed. V2C XES supported by DFT calculations provided important insight into the chemical nature of the species adsorbed on Fe sites. The unique combination of techniques applied under realistic reaction conditions and the corresponding catalytic data unraveled the adsorption of ammonia via oxygen on the iron site. The derived reaction model supports a mechanism where adsorbed NO_x reacts with ammonia coordinated to the Fe^{3+} site yielding Fe^{2+} whose reoxidation is slow.

INTRODUCTION

Fe-ZSM-5 is one of the most widely studied zeolite catalysts for the selective catalytic reduction of nitrogen oxides (mostly NO [1]) by ammonia (NH_3-SCR) [2-5]. This process is employed as an important part of exhaust aftertreatment systems of diesel vehicles with metal exchanged zeolites extensively used for automotive applications [1,6,7]. The mechanistic insight is required as a basis for kinetic models of the process which are needed to design and model the aftertreatment system. Iron is known to be the required active component of Fe-zeolite catalysts for NH_3-SCR and demonstrates the possibility of coordinating not only NO_x [8,9] but may also adsorb ammonia [10] and water [11]. Hence, both catalyst development and application require detailed knowledge of processes taking place on the active Fe sites and the identification of both structures of Fe sites and adsorbed species under relevant conditions.

There have been several attempts to reveal the mechanism of NO_x removal by NH_3-SCR over Fe-containing catalysts [4,12-14] with respect to the formation of the Fe^{2+} site [15], which is important since reoxidation of Fe^{2+} to Fe^{3+} is a slow step in SCR [13-15]. Two commonly proposed mechanisms involve oxidation of NO to form adsorbed NO_x catalyzed by Fe sites. The resulting intermediate then reacts with NH_4^+, which can be adsorbed on both Fe sites and on zeolite, to form ammonium nitrite (NH_4NO_2) which is then decomposed to nitrogen and water. Metkar *et al.* [12] suggest that the reaction of NO_x and NH_4^+ takes place on Fe^{3+} sites with the subsequent desorption of N_2 and H_2O from an Fe^{2+} site, whereas Ruggeri *et al.* [13] propose spillover of NO_2 formed on an Fe^{3+} to the zeolite, releasing an Fe^{2+} site. NO_2 then reacts with NH_4^+ on the Brønsted acid site of the zeolite.

Alternatively, it has been suggested that first an NH_3 molecule adsorbs on an Fe^{3+} site [16] resulting in Fe^{2+}-NH_2. NO then reacts with this Fe amide complex yielding nitrogen, water and releasing Fe^{2+} which is later reoxidized by O_2 to the initial Fe^{3+}. Reoxidation of the Fe sites is considered to be the rate-determining step of SCR in this case [10].

Proof of the suggested mechanisms requires a careful description of the local coordination of the catalytic Fe sites in Fe-ZSM-5 under reaction conditions. Traditional spectroscopic techniques like *in situ* IR and UV-Vis [17] do not allow unambiguous determination of adsorbed NO_x and / or NH_x on the iron sites as contributions of those are small relative to the NO_x and NH_x adsorbed on zeolite matrix. The task becomes even more demanding with addition of water to the system, which is inevitable as it is one of the reaction products, competes for adsorption sites with ammonia[18] and strongly influences the catalytic performance of SCR catalysts [19-22]. Most *in situ* IR and UV-Vis studies have, however, been reported without the addition of water, also in spite of the evidence of different NO_x adsorption dynamics during SCR

by hydrocarbons obtained by *in situ* IR with and without water vapor [23]. In-situ Mössbauer spectroscopy is another tool to study Fe sites with the possibility to reveal the oxidation state and coordination geometry of the sites [24,25]. The technique requires ^{57}Fe enriched samples which imposes a requirement to synthesize the sample specifically having in mind Mössbauer spectroscopy and makes the task more complicated [26]. Mössbauer spectroscopy can be performed *in-situ* [27] and *operando* [28] but is more often used to characterize quenched (freeze-trapped) intermediates [29].

An attractive alternative are synchrotron-based techniques which have demonstrated their ability to shed light on the local coordination environment of transition metals [30-32]. Among these tools X-ray absorption spectroscopy (XAS) is one of the most established techniques allowing to selectively probe the local chemical environment of the transition metal of interest. Herein we focused on the local chemical environment of Fe species in a zeolite matrix. The different regions of a XAS spectrum supply complementary structural information, the analysis of the pre-edge and the X-ray absorption near-edge structure (XANES) regions can be correlated to the oxidation state(e.g. Fe^{2+} or Fe^{3+}) and geometry (e.g. Fe tetrahedral or octahedral), this task can be accomplished either by comparing the unknown spectrum with references compounds, or by the use of calculated spectra [33-38]. Additionally, the study of the extended X-ray absorption fine structure (EXAFS) may result in a detailed description of atomic neighborhood of a targeted element, information on the chemical nature of ligands, bond distances and structural disorder can be obtained by refining the experimental spectrum to a calculated one [37]. In spite of its many advantages, XAS cannot distinguish between atoms with close atomic numbers, e.g. one could not differentiate O from N in the chemical neighborhood of Fe. Also adsorbed species and poor scatterers such as light elements are difficult to detect [39].

This limitation may be overcome using emerging X-ray photon-in / photon-out techniques such as high energy resolution fluorescence detected X-ray absorption spectroscopy (HERFD-XAS) and X-ray emission spectra (XES) [30-32,40]. These techniques explore the relaxation processes after a core hole is created due to the absorption of an X-ray photon. The detection of XAS spectrum in HERFD mode allows enhancing spectral features in the pre-edge and XANES regions, leading even to the identification of adsorbed species on catalytic sites [41]. In its turn, XES technique examines in depth the electronic structure of a certain element (for details, cf. [42,43]). The XES spectrum can be divided in several regions, hereafter we especially exploit the valence-to-core transition region (V2C, referring to the satellite emission lines Fe Kβ" and Fe $K\beta_{2,5}$) . Such lines correspond to transitions of electrons in occupied valence orbitals, which fill the 1s core hole created during the absorption process. These electrons may also come from the ligands, and therefore they may carry chemical information on the ligands. Despite present state-of-the art XES data collection is more time consuming than EXAFS, the V2C region allows identifying ligands and bond distances in particular by comparing the measured spectral features to calculated ones [33,44]. Density functional theory (DFT) based methods have been successfully employed in the calculation of XES spectra and structural models are built based on prior knowledge [32,44].

The inherent advantage of all these complementary techniques is their application under working conditions of the catalysts (i.e. *operando*) due to the penetration ability of hard X-rays, e.g. by using a quartz capillary microreactor with a plug-flow reactor geometry [45]. This allows a correlation of the catalytic performance with the structure of the active sites (XAS) and the adsorbed species (V2C XES). There are only a few studies in this direction exploring *in situ* the V2C region to investigate catalysts [46]. One of the authors of the present work employed V2C XES to study adsorption of water and NH_3 on Ti in an *in-situ* pretreated zeotype catalyst [47]. Recently, a XES experiment was reported on the adsorption of NH_3 on copper sites of the Cu-SSZ-13 zeolite [48], as the shift of the Cu Kβ" feature to higher energies supported the formation of the Cu-N bond as evidenced in earlier studies. However, the real challenging goal is to identify the structure of the active species also under operating (*operando*) conditions, as extensively done in catalysis in recent time (e.g. refs. [49-56]). Compared to *in situ* studies, in which the reaction conditions such as temperature, gases and catalyst loading are adapted to make the measurement possible, *operando* spectroscopy results in measuring the catalytic activity at the same time as acquiring the spectra [57-61].

In this work we probe, to our knowledge for the first time, the structure of the iron sites in Fe-ZSM-5 under *operando* conditions using high-energy-resolution fluorescence-detected (HERFD) XANES [62,63] combined with V2C XES. The Fe K-pre-edge peak from the HERFD-XANES spectra and Fe Kβ" V2C lines from the X-ray emission spectra [48,64] were used to gain information on the oxidation state, coordination number and the chemical nature of the ligands on the Fe sites in the Fe-ZSM-5 catalyst during NH_3-SCR of NO in the presence and absence of water and under other related reaction conditions using information from DFT calculations. The gained results are used to validate the mechanism of NH_3-SCR of NO over Fe-ZSM-5 and in particular to identify some of the possible intermediates of this reaction.

EXPERIMENTAL

The Fe-ZSM-5 catalyst was prepared by liquid ion-exchange of NH_4-ZSM-5 zeolite (Si/Al = 11, Clariant) with $FeCl_2$ [65]. For this purpose, 5 g of zeolite was stirred in 500 mL of a 0.05 M $FeCl_2$ solution under N_2 flow for 24 hours. The resulting solid was filtered, dried for 2 hours at 120 °C, and calcined for 5 hours at 550 °C in static air. The final Fe concentration as measured by AAS was 1.3 wt%. For the catalytic experiment the sample was pressed, crushed and sieved to obtain a fraction with 100 – 200 µm (200 – 300 µm for the laboratory test bench) grains. The catalytic data taken on the laboratory bench are given in the electronic supporting information (ESI).

The XAS/XES measurements were carried out at the European Synchrotron Radiation Facility (ESRF, Grenoble, France) at the high-resolution X-ray spectroscopy beamline ID26 equipped with three mechanically independent undulators providing a flux of 10^{13} photons per second at the sample. A cryogenically cooled Si (111) double-crystal monochromator was used for selecting the photon energy. The emission spectrometer was equipped with five Ge (620) analyser crystals, spherically bent (r = 1 m) and installed in a Rowland geometry with respect to the sample and the detector. The counts of the avalanche photo-diode detector were normalized by a photodiode between the slits and the sample. The resulting instrumental energy bandwidth in terms of the FWHM (full width at half maximum) of the elastically scattered beam at 7113 eV is 1.4 eV, which is enough to resolve the Fe Kβ-lines and is slightly greater than the Fe K-edge spectral broadening. This is nevertheless no obstacle for clearly resolving the pre-edge features: due to the high-resolution detection these transitions are well-separated from the main edge onset and require minimal or hardly any extraction [66]. The beam size was kept as 1 mm x 4 mm to avoid formation of hot spots due to heating by a smaller localized focused beam.

The X-ray absorption spectra in terms of HERFD-XANES were measured by scanning the incident energy and detecting the fluorescence at the maximum of the Fe $K\beta_{1,3}$ emission line (e.g. at 7058.81 eV). The pre-edge integrated intensity and centroid position were calculated from the fitted peaks, omitting contributions centered above 7115.6 eV [35].

The X-ray emission spectra around the main ($K\beta'/K\beta_{1,3}$) emission lines and the satellite ($K\beta''/K\beta_{2,5}$) lines were recorded between 7010-7140 eV while applying an excitation energy of 7145 eV, far beyond the detected emission energy range in order to avoid the elastic scattering line and resonant excitations in the spectra. The error introduced by the background extraction (described in detail elsewhere [39,42] and in the ESI) has been expressed by the fit residual between the experimental tail and the fitted one and is in the range of 3%. To check the reproducibility of the XES measurements we remeasured some spectra using a different catalyst batch. The normalized spectra matched each other. It should be additionally noted that no drift in the beamline components was observed during the experiment.

A heated quartz capillary microreactor (diameter 1 mm, wall thickness 0.02 mm) served as both plug-flow reactor and an *in situ* cell [67]. The microreactor was mounted on top of an air flow furnace (Gas Blower GSB-1300, FMB Oxford), positioned at the focus of the spectrometer at 45° with respect to the incident beam and the analyser crystal assembly. Pure gases and gas mixtures were dosed to obtain the desired volume concentrations: 1000 ppm NO, 1000 ppm NO_2, 1000 ppm NH_3, 5% O_2 and pure He as balance. Water vapor (~ 1.5% H_2O) was dosed via a saturator. The gas flow was kept at 45 mL/min and GHSV = 130 000 h^{-1}. Pfeiffer Vacuum Thermostar GSD 320 T1 quadrupole mass spectrometer was used for the online gas analysis. Conversion (X) of NO was defined using values of ion current of m/z 30 measured in the outlet of the microreactor capillary and in the bypass line as $X=(1-I_{reactor}/I_{bypass})$. The temperature of the microreactor was kept by the Gas Blower at 255 °C without the X-ray beam (verified by the external thermocouple) but changed due to heating by the beam. This heating cannot be measured directly but is deduced from the increase of NO conversion from ca. 49% to ca. 62% after opening the beam shutter (Fig. S4). From the comparison of the given values of NO conversion with the laboratory bench data (Fig. S3) the catalyst bed temperature under X-ray beam is estimated to be approximately 295 °C. The same approach was previously used to determine the real bulk temperature of catalysts under working conditions in the DRIFTS *in situ* cells [68]. The NO conversions reported in the current paper were measured with an open X-ray shutter (the beam on). The transferability of the catalytic data between the microreactor capillary and laboratory setups was proven to be valid for the particular reaction and the particular catalyst beforehand [69].

In the beginning of measurements and during changing from experiments with highly adsorbing gas species (NH_3, H_2O) to the experiments without them the catalyst was flushed with He for 15 min at 550 °C. After experiments involving NO_x only the catalyst was flushed with He for 15 min at 450 °C. The whole experiment was planned in order to minimize the number of flushing steps and the total exposure to 550 °C was 1 hour. The named conditions are milder than those reported to alter Fe sites significantly (i.e. "steaming" at 650 °C [70] or hydrothermal deactivation [71-73] and formation of "α"-sites catalyzing N_2O decomposition[11,24,74]). It should be noted that the measurements comprised acquisition of many spectra in series with their subsequent averaging and the spectra did not show any changes in the sample during long measurements. Therefore we assume that the state of the catalyst (especially, Fe sites) did not change during the measurements.

For the simulation of X-ray emission spectra, the structures of molecular models were optimized with the ADF 2013.01 program package [75,76] using density functional theory (DFT) with the BP86 exchange-correlation functional [77,78] and a TZP basis. The X-ray emission spectra were then calculated with the ORCA 2.9.0 [79] program package using single point DFT calculations [44] with the BP86 exchange-correlation functional [77,78] and the def2-QZVPP basis set [80]. The considered structures are based on a commonly used model for a single iron pocket within the zeolite pore [16,81,82]. The spectra were convoluted using a Gaussian line shape with a FWHM of 1.5 eV. All plotted spectra are shifted by 179.71 eV to align them with the experimental spectra [83].

RESULTS & DISCUSSION

Structure of the used Fe-ZSM-5 catalyst and its catalytic performance

Designing catalysts with Fe sites of the same type is an important prerequisite for a successful data analysis since XAS/XES techniques result in an averaged response from all Fe atoms in a studied system, i.e. the state of all types of Fe atoms in the probed system will be averaged. As Fe may be incorporated in zeolites in form of many different species [70,84] (isomorphously substituted framework sites, extraframework single-Fe, binuclear, oligomeric Fe_xO_y and Fe_2O_3 species) it is of utmost importance to make sure that the catalyst under consideration has only one type of Fe sites. Mononuclear extraframework Fe complexes show the highest activity in NH_3-SCR [15,21,84] and, therefore, the Fe-ZSM-5 catalyst studied here was prepared by liquid ion-exchange with $FeCl_2$ aiming mainly at monomeric and not binuclear or clustered Fe sites which was confirmed by UV-Vis and EXAFS [15] (Figs. S1 and S2 respectively). Our conventional EXAFS analysis (similar to refs. [85,86]) combined with pre-edge analysis using HERFD-XANES data uncovered that the local chemical environment of Fe in the as-prepared Fe-ZSM-5 catalyst can be best described as a FeO_x (x = 5) moiety. No conclusion could be made about the nature of further coordination shells from the EXAFS results. However, from the preparation procedure one can assume that the Fe atoms are not incorporated into the zeolite structure, in accordance with [87] but are located in the zeolite cationic sites [4,82] as defined by the used synthesis conditions [65].

The conversion of NO during NO oxidation and SCR of NO with and without water in the in situ microreactor cell are given in Fig. 1 and the catalyst performance measured using the laboratory test bench can be found in Fig. S3. The mass spectrometer at the beamline was not calibrated for NO_2 and N_2O but in the laboratory test bench less than 5% NO were converted to NO_2 and less than 1% to N_2O under the same conditions. As noted for the same setup in our previous work, the catalytic data measured at the beamline corresponds well to the data obtained in the laboratory [69]. Moreover, the catalytic activity of the synthesized catalyst is similar to activity of a commercial Fe-BEA zeolite [69].

We report the activity of Fe-ZSM-5 catalyst in two reactions, namely NO oxidation and SCR of NO because there is an ongoing debate in literature whether the rates of these reactions are correlated [88] or not [89]. The effect of water on the two reactions is similar. NO oxidation is strongly inhibited [19], SCR of NO with water still demonstrates a high conversion but lower than without water [88]. Another important aspect is that no full conversions are achieved under the conditions of an experiment, i.e. the reagents present in the whole catalytic bed and there are, thus, no parts of the reactor not exposed to the reagent species.

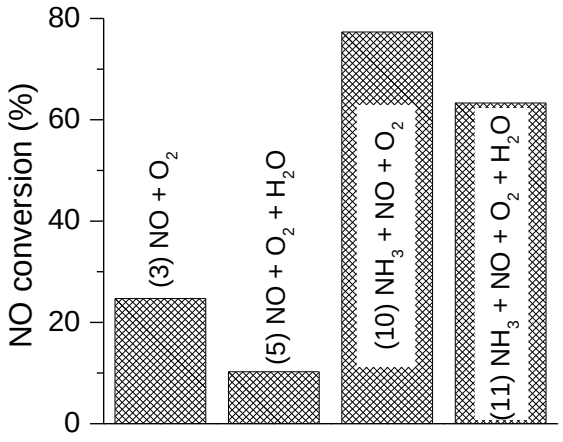

Figure 1. Conversions of NO measured during XAS/XES data acquisition for NO oxidation and SCR of NO with and without water. Conditions: 1000 ppm NO, (1000 ppm NH_3), 5% O_2, (approx. 1.5% H_2O) and pure He as balance.

Dynamics of the oxidation state and coordination of iron studied by analysis of the Fe-K absorption pre-edge

In order to gain information on the geometry and the oxidation state of Fe sites under different reaction conditions, pre-edge spectral features in the XANES spectra, collected with high energy fluorescence were analyzed. For this purpose, the emission line with instrumental resolution (~1 eV) far below its lifetime-broadening (4.5 eV for the Fe $K\beta_{1,3}$) was selected. This acquisition mode presents two main advantages compared to transmission XAS and conventional fluorescence detection: i) the energy resolution of the spectral features of the pre-edge in the XANES region is highly improved [85,86], ii) the HERFD detection mode allows selecting one specific channel of decay leading to a XAS spectrum with chemical and/or spin selectivity [90,91]. We have used the $K\beta_{1,3}$ line which arise when a 3p electron decays to fill a 1s hole (3p to 1s electronic transitions) [90,91]. Since the 3p hole in the final state strongly interacts with the spin of the 3d electrons spin selectivity is observed as previously shown [92,93]. The 3p electrons are more prone to the influence of the chemical environment because the energy levels are closer to those of the ligand orbitals and the interaction is stronger. Hence, we mainly exploited the chemical sensitivity of the $K\beta_{1,3}$ lines which have been previously used in site selective XAS measurements [94,95] and neglected the spin selectivity.

Fig. 2 shows the HERFD-XANES spectra in the Fe-K pre-edge region during the different model and SCR reaction conditions. The full HERFD-XANES spectra are presented in the ESI (Figs. S5 and S6). Moreover, Fe-K pre-edge spectra of reference compounds are shown in Fig. S7 (ESI).

In the next step we used analogously to Wilke et al. [35] a graphical correlation of the Fe coordination geometry and oxidation state to the pre-edge peak integrated intensity (area) and centroid position (area-based average position). The resulting plot of the observed pre-edge intensity against the centroid position is shown in Fig. 3 including a grid of data points of reference samples with known Fe geometry and oxidation state (staurolite for Fe^{2+} T_d, olivine for Fe^{2+} O_h, $FePO_4$ (rodolicoite) for Fe^{3+} T_d and hematite (α-Fe_2O_3) for Fe^{3+} O_h) and trends resulting in binary mixtures (80:20, 60:40, 40:60 and 20:80) of these four states. The data points extracted from the *operando* XANES (Fig. 2, corresponding catalytic data in Fig. 1) of the Fe-ZSM-5 catalyst under reaction conditions are superimposed onto this trend-grid and marked with the experiment number (Table 1). Generally, when exposed to oxidizing conditions (involving O_2, H_2O, NO and NO_2) the Fe is present as Fe^{3+}, addition of NH_3 to these mixtures results in a slightly decreased average Fe oxidation state. When NH_3 alone is fed (exp. 6 and 7) a large fraction of Fe is reduced to Fe^{2+}.

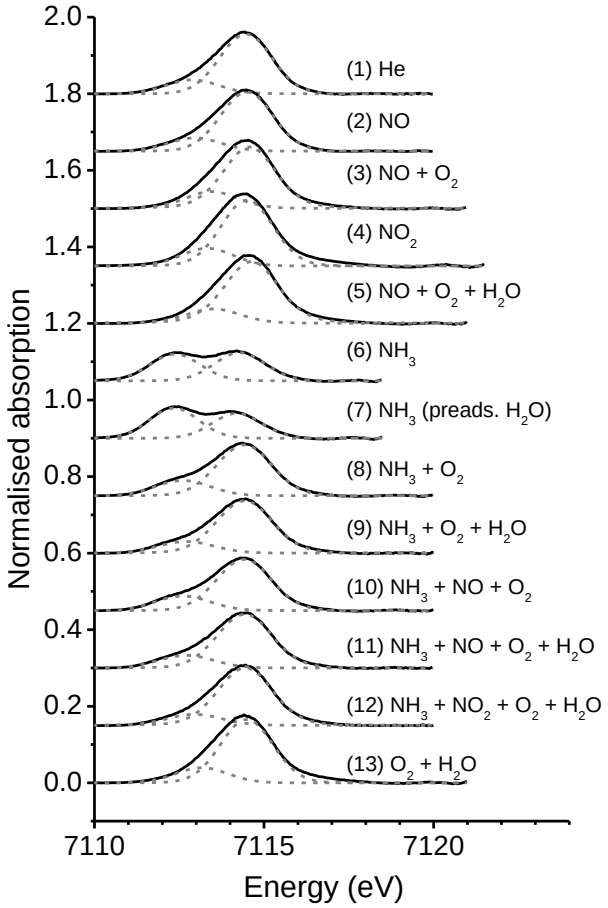

Figure 2. HERFD-XANES spectra of Fe-ZSM-5 catalyst under model and SCR reaction conditions (cf. Table 1) recorded in the pre-edge region of Fe-K absorption edge.

The data points present a trend showing the change of oxidation state and the number of ligands in the coordination sphere of Fe atoms in the Fe-ZSM-5 catalyst system. The points trace a curve from Fe^{2+} approximately halfway in between T_d and O_h geometries to Fe^{3+} in T_d geometry. The state of the Fe^{2+} species can be regarded either as mixture of T_d and O_h geometries (coordination numbers 4 and 6 respectively) or a different local geometry with coordination number of ca. 5. The pre-edge analysis supports both cases but cannot differentiate between them [35,36]. Potentially, the multiplet structure in the pre-edge spectra (Fig. 2) can be used which goes beyond the scope of this work [96].

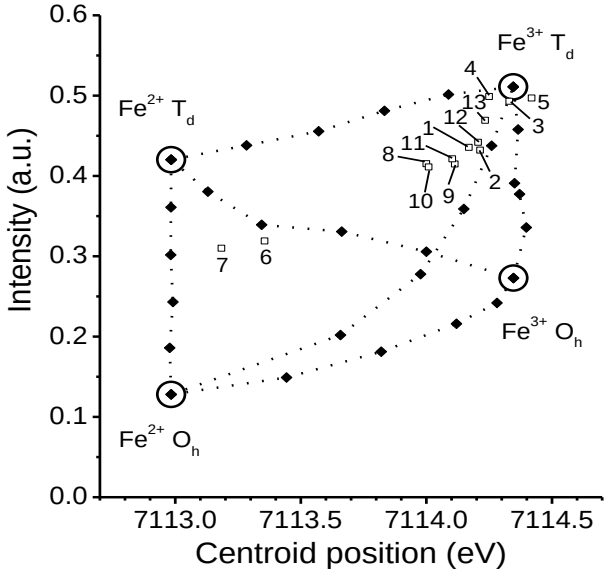

Figure 3. Plot of the pre-edge integrated intensity (area) and the centroid position (area-based average position) extracted from HERFD-XANES spectra of reference compounds representative of Fe^{2+} and Fe^{3+} in O_h and T_d states (large circles), their binary linear combinations (filled diamonds) and the Fe-ZSM-5 catalyst under reaction conditions numbered according to Table 1 (open squares) used to estimate Fe oxidation state and coordination geometry.

The analysis of the Fe-K pre-edge features (Fig. 2) reveals a strongly dynamic chemical state between Fe^{3+} and Fe^{2+} which depends on the reaction conditions. The coordination number in the first coordination shell of Fe is 4 during the exposure to oxidizing conditions (O_2, H_2O and NO_2 in exp. 3, 4, 5 and 13), 5 during the exposure to strongly reducing conditions (6 and 7), and between 4 and 5 under SCR conditions and after adsorption of pure NO. However, such an analysis does not provide any information about the nature, or chemical identity, of the species surrounding the Fe atoms.

Chemical speciation of the local coordination sphere of Fe by valence-to-core spectroscopy under reaction conditions

Complementary to the pre-edge analysis and EXAFS data, V2C XES has been used to gain insight to the type of neighboring atoms. The Kβ" and $K\beta_{2,5}$ regions have a high chemical sensitivity, since the corresponding electronic transitions originate from the ligands to fill the Fe 1s core hole [33,43,44]. The environment of Fe sites in Fe-ZSM-5 was probed under different gas compositions used to represent SCR of NO, SCR of NO_2, NO oxidation and NH_3 oxidation in the presence or absence of H_2O. Also the influence of adsorption of individual gases (NO, NO_2, NH_3 and H_2O) on the chemical environment of Fe was evaluated.

Table 1. Experimental conditions, oxidation state, and local coordination number estimated by the pre-edge spectra and the qualitative description of the Kβ" V2C region. The gas compositions are named herein according to the reactive gases in the gas mixtures.

Exp. Nr.	Gas composition	Fe oxidation state	Fe coord. number	XES peaks (eV) A 7088	B 7092	C 7097
1	He	2.8-3.0	4-5	-	+	-
2	NO	2.8-3.0	4-5	+	+	-
3	$NO+O_2$	3.0	4	+	+	-
4	NO_2	3.0	4	+	+	-
5	$NO + O_2 + H_2O$	3.0	4	+	+	-
6	NH_3	2.2-2.4	5	+	+	+
7	NH_3[a]	2-2.2	5	+	+	+
8	$NH_3 + O_2$	2.6-2.8	4-5	+	+	±
9	$NH_3 + H_2O + O_2$	2.6-2.8	4-5	+	+	±
10	$NO + O_2 + NH_3$	2.6-2.8	4-5	+	+	+
11	$NO + O_2 + NH_3 + H_2O$	2.6-2.8	4-5	+	+	±
12	$NO_2 + O_2 + NH_3$	2.8-3.0	4-5	+	+	-
13	$O_2 + H_2O$	2.8-3.0	4	-	+	-

[a] Fe-ZSM-5 with preadsorbed H_2O (after exp. 13 without flushing by He)

First, adsorption of NO_x on Fe sites of Fe-ZSM-5 was investigated. For that purpose, both pre-edge and V2C spectra were recorded and analyzed for the following gas media: NO, $NO+O_2$, NO_2, and $NO+O_2+H_2O$ (Table 1, exp. 2-5). All V2C spectra measured under these conditions were virtually identical in the $K\beta_{2,5}$ region (Fig. 4). The $K\beta_{2,5}$ features of those spectra were in turn the same as those for Fe-ZSM-5 measured under He. Pre-edge analysis shows almost the same oxidation state 3 (very slightly reduced 2.8 – 3 for NO/He feed) for all NO_x-containing mixtures. The presence of water does not show any notable effect on NO_x adsorption contrary to ref. [23]. Notably, adsorption of pure NO (without O_2) results in a different coordination geometry than that for NO_2 or NO + O_2 mixtures, i.e. the HERFD-XAS data point of the experiment 2 in Fig. 3 is significantly shifted towards O_h geometry compared to other experiments involving NO_2 or NO + O_2 (exp. 3,4, and 5). The fact that adsorption of pure NO slightly reduces Fe and leads to the increase of the coordination number supports the NO oxidative activation process suggested in refs. [12,13], given as reaction (1),

$$Fe^{3+}\text{-}OH + ON^{\cdot} \leftrightarrow Fe^{2+}\text{-}O^{+}H\text{-}N{=}O, \qquad (1)$$

which proceeds via Fe nitrosyl intermediate accounting for the slightly higher observed coordination number. Different mechanisms of adsorption of NO and NO_2 (or NO + O_2) are in line with the IR studies [97].

The structure with three-coordinated positively charged oxygen is further supported by the analysis of the emission lines in the low-energy region of the V2C spectra (Kβ") in combination with DFT calculations, as is discussed in the following.

For indentifying the broad overlapping peaks with low intensity, the second derivative of the V2C spectra (Fig. 5) was analyzed. The XES spectra before background extraction were used for this analysis as the background extraction may introduce a significant error in the Kβ" spectral region. The second derivative of the Kβ" feature (7080-7097 eV) comprised up to three peaks at

ca. 7087, 7092, and 7097 eV which herein have been assigned as peaks A, B, and C, respectively. While for the catalyst under He and O_2 (experiments 1 and 13) only peak B is present, the additional peak A appears for all NO_x-containing mixtures.

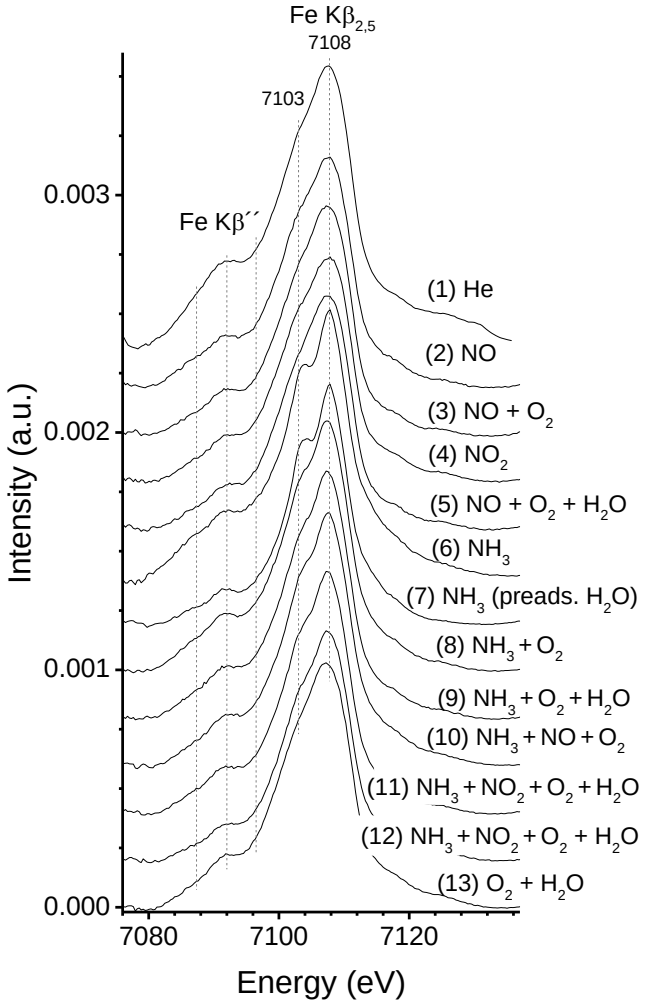

Figure 4. Comparison of measured V2C spectra of Fe-ZSM-5 in different gas media (cf. Table 1).

As a second step, interaction of Fe sites with NH_3 was probed by analyzing Fe-ZSM-5 catalyst under an atmosphere of NH_3, NH_3+O_2, and NH_3+H_2O+O_2 (exp. 6 – 9). The interaction of dehydrated Fe with NH_3 without O_2 (exp. 6) leads to a significant change of the V2C spectrum. A splitting of the K$\beta_{2,5}$ peak into two peaks with maxima at 7103 and 7108 eV (Fig. 4) is observed. At the same time, the pre-edge analysis points to a reduction of Fe^{3+} to Fe^{2+}. Repetition of the same experiment with Fe-ZSM-5 after adsorption of H_2O (exp. 7) still yielded peak splitting in the K$\beta_{2,5}$ region, though less pronounced. Interaction of the catalyst with NH_3 and O_2 (without or with H_2O, exp. 8 and 9) resulted in spectra similar to the spectra of adsorbed NO_x but with a shoulder at 7103 eV, while the pre-edge analysis yields an oxidation state of iron 2.6-2.8.

If NH_3 is present in the feed, the analysis of the Kβ" region shows both peaks A and B. Thus, peak A appears when either NH_3, NO or NO_2 are present in the feed, which is most likely indicative of the formation of Fe-$O^{\delta+}$H-N- intermediate (see below). Peak B is always present, whereas peak C is clearly observed upon NO-SCR reaction conditions without water (experiment 10) and under NH_3 flow (experiments 6 and 7). The presence of the peak C under other NH_3-containing feeds cannot be confirmed because of low intensity, below the noise level. In this case we marked the peak C as ± in Table 1. We assign this peak C to a direct NH_3 adsorption [48] on Fe. This is supported by the strong reduction of Fe (Fig. 3) and to the reported strong affinity Fe sites in this catalyst to NH_3 which may lead to the inhibition of SCR reactions by NH_3 (top row of the Scheme 1) [69].

DFT calculations of V2C XES spectra

To assign these peaks and identify the nature of the ligands on Fe, we performed DFT calculations of the V2C XES spectra of several molecular models (Fig. 6). The K$\beta_{2,5}$ region can be assigned to transition from ligand 2p-orbitals, whereas the Kβ" region is due to transitions from the ligand 2s-orbitals [33,43,44]. The latter are mainly contributing to the oxygen and nitrogen lone pairs.

For the K$\beta_{2,5}$ region, calculated spectra of selected models are shown in the ESI. Here, we cannot assign the appearance of the peak at 7103 eV based on the DFT calculations, but conclude that its description requires the use of more sophisticated models of the zeolite framework.

On the other hand, for the Kβ" region, the DFT calculations provide a clear assignment. The calculated spectra are shown in Fig. 6, alongside the orbitals from which the main contributing transitions originate. For model (1), in which two hydroxyl ligands are coordinated to the iron site only peak B is found in the Kβ" region. It can be assigned to a transition originating from the oxygen lone pairs of hydroxyl ligands and of oxygen atoms in the zeolite framework. In model (2), one hydroxyl group is replaced by a -O^+H-NH_2 ligand to mimic a proposed intermediate with partially positively charged, three-coordinated oxygen. In this case, peak A appears in addition to peak B and it can be assigned to transitions from the lone pairs of the oxygen carrying a partially positive charge. For model (3), in which both a hydroxyl and a NH_2 ligand are coordinated to the iron site, peaks B and C are present, whereas peak C is due to transitions from the nitrogen lone pairs of the NH_2 ligand. This peak C is also present for models (4)–(5), in which the iron site is coordinated by one NH_2 ligand and one NH_2 or NH_3 ligand. However, it disappears for model (6) with two NH_3 ligands, because there are no nitrogen lone pairs. For the models (4)–(6), which have no hydroxyl ligands, the intensity of peak B decreases, but it remains present because of the contributions of oxygen lone pairs of the zeolite.

The second derivative of the spectrum calculated for model (2), in which all three peaks are present, is included in Fig. 5. Additional calculations to support our assignment are included in the ESI. In particular, we can show that the assignment is independent on the oxidation state of the iron atom, information that is also supported by the pre-edge data.

In summary, the DFT calculations support the assignment of peak A to the formation of Fe-$O^{\delta+}$H-N- intermediate (where N can originate from NO or NH_x). Moreover, peak C can be clearly assigned to the coordination of ligands with nitrogen lone pairs, in accordance with [48]. Thus, as spectra 2-5 for feeds containing NO_x (Table 1) show peaks A and B and no peak C, we can suggest NO

adsorption on Fe only via $O^{\delta+}$ atom from the hydroxyl group, e.g. as Fe^{2+}-O^{+}H-N=O, similar to one of the structures reported in [16].

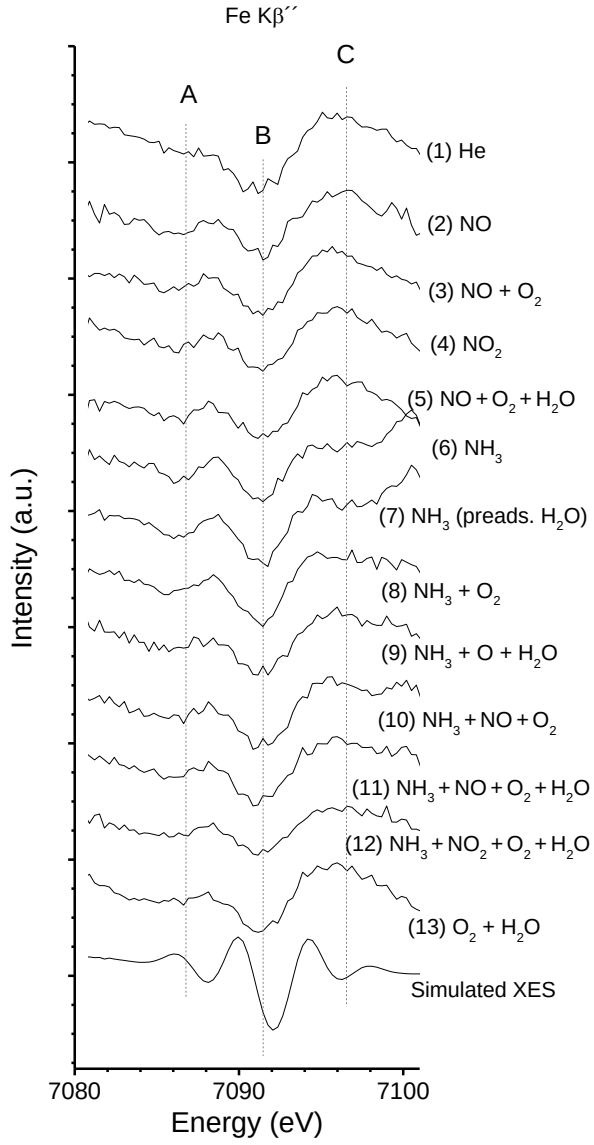

Figure 5. Comparison of the second derivatives of the V2C spectra (Fe Kβ" lines) of Fe-ZSM-5 in different gas media (cf. Table 1), the simulated XES was obtained as the second derivative of the calculated spectrum of the structure (2).

Insight into the mechanism of NH_3-SCR of NO and discussion on the operando spectroscopic results

Analysis of the weak emission lines in the Kβ" region V2C XES spectra can identify the existence of O, three-fold coordinated $O^{\delta+}$ and N atoms in the first coordination shell of Fe sites (Fig. 6 and Table 1). The three-fold coordinated $O^{\delta+}$ feature seems to exist in all recorded spectra involving NO_x and / or NH_3 and the feature due to the N atom is only clearly seen for adsorbed NH_3 and SCR of NO without water (less clear for SCR of NO with water), i.e. Fe-NH_x coordination seen by IR spectroscopy [10,13,97,98] can be severely hindered due to competition with water under real SCR conditions. Water is known to occupy Lewis acid sites of the zeolite in the presence of ammonia [18] and also to adsorb on Fe sites [11], and a high partial pressure of water vapour can indeed completely suppress the direct coordination of NH_3 to Fe. The catalytic data (Fig. 1) confirms the inhibiting effect of water for both NO oxidation (exp. 3 and 5) and SCR of NO (exp. 10 and 11). At the same time with water the intensity of the peak C decreases below the noise level. Hence, even if there is any X-ray emission in the peak C region, this may be due to N from $Fe^{(3-\delta)+}$-$O^{\delta+}$H-NH_2 moiety. This species (top right in the Scheme 1) may be the ammonia intermediate along with the structure representing nitrous acid adsorbed on Fe site [16] (middle right of the Scheme 1). Without water peak C (clearly observed in this case) may be due to the direct coordination of NH_x on Fe [48] (Scheme 1, top left). Therefore, as water suppresses peak C and also inhibits NO conversion we suppose that a NH_x directly coordinated on Fe sites is the real intermediate [16] and is not observed due to the fast consumption (and also the competition with water). $Fe^{(3-\delta)+}$-$O^{\delta+}$H-NH_2 moiety (Scheme 1, top row) exists under only NH_3 conditions and may also exist under SCR conditions (triple-coordinated O^{+} is observed upon adsorption of both NH_3 and NO) but is not quickly consumed and is not involved in the fastest reaction pathway.

According to the HERFD-XANES data, under exposure to water vapor (Table1, exp. 13) Fe sites show coordination number 4 which is below the maximum observed coordination number 5 (under NH_3 atmosphere) but still leads to an inhibition of SCR. This strongly hints to a Langmuir-Hinshelwood mechanism [69], on a single Fe site, for which the site must have two coordination vacancies or two neighboring Fe sites (which is excluded in our case). If even one of the coordination vacancies is occupied the inhibition would be observed.

The actual pathway of SCR of NO with the intermediates suggested in our study is shown as the middle and bottom lines of the Scheme 1. Adsorption of NO may take place on the Fe^{3+} site with partial reduction of this site which fits with [13] and then followed by adsorption of ammonia (an intermediate was suggested in the DFT study [16]). Since the adsorption of NH_3 is the reversible process and water is the product high partial pressure of water may inhibit this stage of the SCR of NO. The nitrous acid and ammine ligands then react together yielding N_2 formation and Fe^{2+} site with lower coordination [69]. HERFD-XANES observed between 20% and 40% of the Fe sites in the Fe^{2+} state during NO-SCR and earlier we observed up to 50% of Fe^{2+} sites by spatially-resolved XAS [69]. The fact that such a high fraction of Fe^{2+} exists under net-oxidizing conditions leads to a conclusion that Fe^{2+} to Fe^{3+} oxidation is slow and possibly the rate-limiting step of NO-SCR [12].

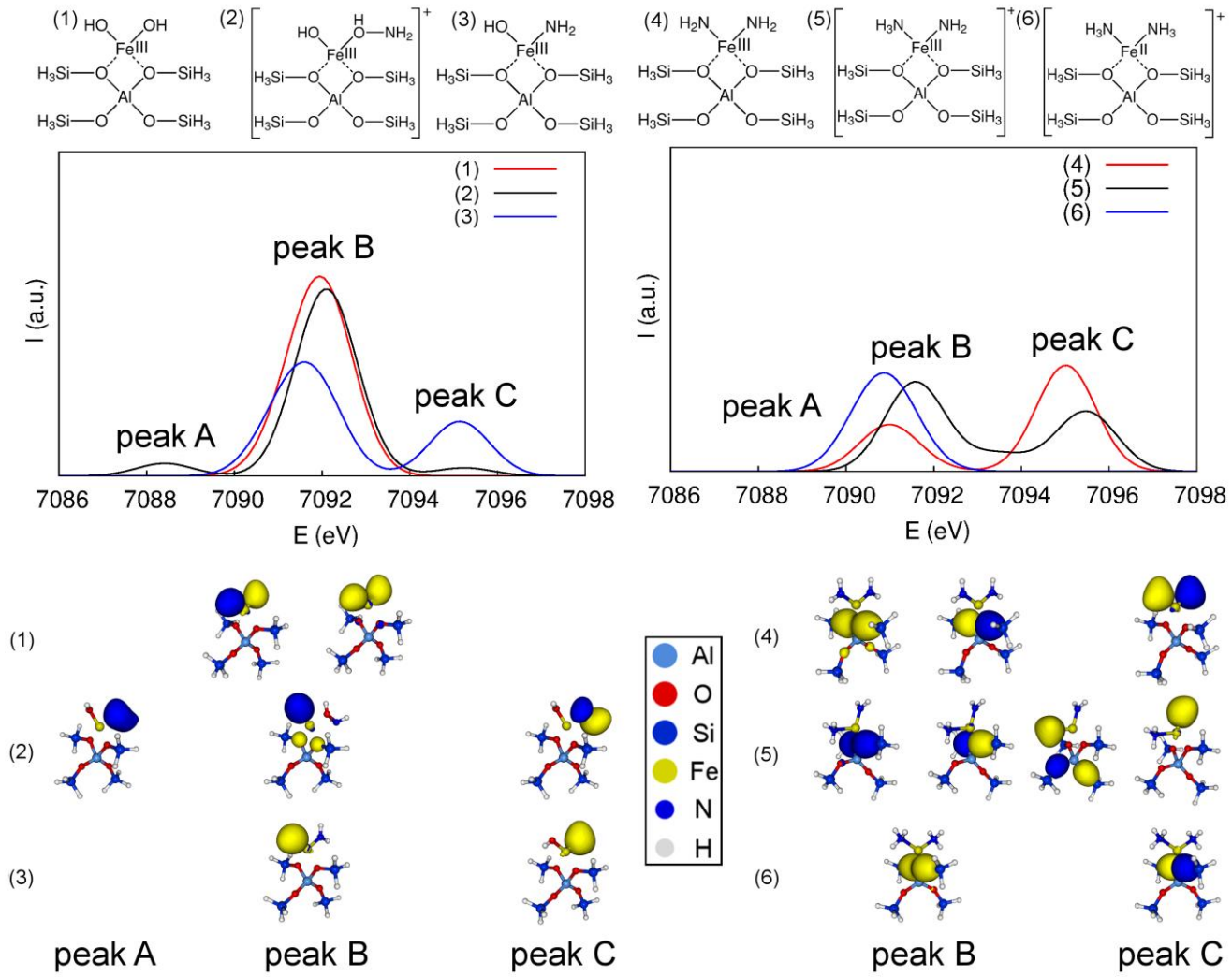

Figure 6. Top: Lewis structures of molecular models (1)-(6) considered in DFT calculations. Middle: calculated V2C XES Kβ" spectra for these models. Bottom: The orbitals from which the main contribution to peaks A-C originates, shown as isosurface plots.

Scheme 1. Suggested intermediates during SCR of NO over Fe-ZSM-5. Additional oxygen coordination (from water or zeolite) in the Fe coordination sphere is left out for simplicity. ZO stands for a zeolite cationic position.

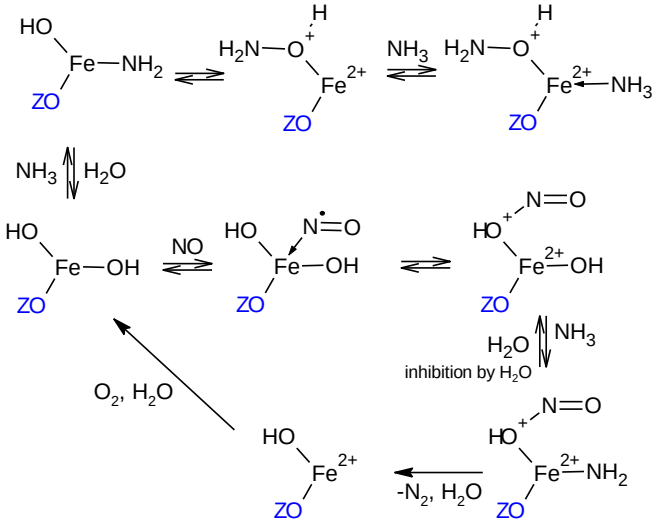

Previous studies by conventional XAS have in agreement with the present here already evidenced dehydration [99] and changes in the oxidation state of Fe sites upon adsorption of NH_3 [15] or during NH_3-SCR (without water) [14]. *Operando* EXAFS revealed changes in the coordination number of Fe sites as a result of SCR and NH_3 adsorption [69]. However, the nature of the adsorbed species could not be unraveled by these techniques. While EXAFS under such disordered system cannot supply information on the third coordination shell of Fe, V2C XES Kβ" spectra is a probe for the ligands and they strongly hint to the presence of an Fe-$O^{\delta+}$H-N intermediate. This can be due to the adsorption of NO but was also observed after adsorption of NH_3 with the subsequent reduction of Fe^{3+} as an alternative to the NH_x ligand in the direct Fe environment. Note that both theory and experiment point out that the contribution stemming from such transition in Fe-NH_x species is weak. Moreover, Fe-NH_x species can also be an actual reacting species which yields very low signal in the spectra because of its quick depletion in the course of SCR. In this case $Fe^{(3-\delta)+}$-$O^{\delta+}$H-NH_2 observed as peak A in the V2C XES spectra can be a precursor for reacting Fe-NH_x or a spectator.

Most importantly, the study was performed using a microreactor with a sieved catalyst to prevent mass transport limitations and to be able to measure catalytic data (but making the spectroscopic experiment more demanding) [59] and a typical SCR feed including water which limits the application of other *in situ* techniques such as FTIR [13,97,98] or EPR spectroscopy [100]. In fact, water is always found in the Fe coordination sphere at temperatures of interest [11]. It competes with ammonia [18] and NO_x for adsorption on the Fe sites and has a profound effect on the catalyst performance [19,88] and, thus, needs to be included in the study. Addition of water resulted in lower intensity of the V2C peak C which decreases the probability of the coordination of an NH_x ligand directly bound to Fe.

Hence, V2C XES - combined with a model catalyst containing a large fraction of monomeric SCR-active iron sites, pre-edge analysis, XANES and EXAFS - is an excellent and presently the only technique to draw a clearer picture of NH_3-SCR mechanism in terms of probing Fe coordination environment under the relevant SCR conditions (a mixture of NO_x, NH_3 and water) and distinguishing between different ligands. This makes it an indispensable complementary tool. A second advantage of V2C XES is that due to its element specific nature we were able to discriminate only those ligands that are within the coordination shell of the probed element, i.e. in the reported case we are monitoring only part of NO_x and NH_x bonded directly to Fe sites and not to the zeolite framework which would have been difficult using other techniques like IR spectroscopy. The third major advantage of V2C is the possibility to vary the geometry of the *in situ* cell, i.e. to choose the plug flow reactor to match reactors normally used for catalyst performance testing. For instance, the shape and design of the in-situ cells for EPR are dictated by resonator cavity, dimensions of which, in turn, depend on the wavelength of microwave radiation used in the specific device [101]. The cells for diffuse reflectance IR and UV-Vis can be constructed using a plug flow reactor geometry [102,103], however, despite DRIFTS is better probing the surface one has to deal with strict space constraints and quantification of the diffuse reflectance data is limited [104-106]. These benefits of the XAS and XES techniques are not only limited to the studied reaction but can also be used for other catalyst systems where predominantly one structural site of the element of interest is present.

Further development of the technique will be a possibility of recording V2C in a spatially resolved way to gain additional information on the catalyst performance and the reaction mechanism depending on the probed catalyst zone [69]. This will require using smaller X-ray beams and result in a smaller number of emitted photons. Higher intensity of the incoming beam will not be an optimal solution for the increasing signal-to-noise ratio as intense X-ray beam will overheat and possibly destroy the catalyst. Therefore, for the spatially resolved XES improved spectrometer design and detector efficiency are needed. The same improvements would allow performing time-resolved XES measurements as another indispensable tool for studying of mechanisms of catalytic reactions in future.

CONCLUSION

Unraveling mechanisms of demanding reactions like NO removal via NH_3-SCR requires studies with defined catalysts under realistic operating conditions in terms of e.g. realistic gas mixtures with water combined with online gas analysis. By the use of complementary X-ray absorption and emission techniques combined with DFT calculations we could confirm several reaction steps speculated in literature and propose a new reaction scheme for the NH_3-SCR of NO over Fe-based zeolites. The results demonstrate that valence-to-core XES as new addition to the "*in situ* toolbox" allows distinguishing between different types of oxygen and nitrogen in the first coordination shell of Fe under *operando* conditions. Thus, together with complementary high resolution XANES and EXAFS [69], it is excellently suited for uncovering the state of the active site and the nearest neighbor environment under SCR conditions or more general of working catalysts. What is more important for studying NH_3-SCR, V2C XES allows specific detection of adsorbed ammonia in the presence of large quantities of water which was previously not possible.

The key reactions in the NH_3-SCR mechanism over Fe-ZSM-5 involve (a) the adsorption of NO and ammonia via oxygen atom on a Fe^{3+} site leading to a partial reduction of the site with (b) subsequent release of Fe^{2+}, nitrogen and water [69], (c) reoxidation of Fe^{2+} as the rate-limiting step and (d) water inhibition by coordination to the active centre. Application of V2C XES Kβ" spectroscopy allowed to evidence the adsorption of ammonia in the presence of water and to elucidate the potential reaction intermediates. The knowledge allows now a more rational catalyst design and facilitates further optimization of this industrially important catalytic reaction.

ASSOCIATED CONTENT

Supporting Information. UV-Vis and EXAFS characterization of the studied Fe-ZSM-5. Catalytic activity. HERFD-XAS data acquisition and pre-edge analysis. XES data acquisition and valence-to-core analysis. HERFD-XANES and V2C XES spectra of the reference compounds. Additional XES calculations. This material is available free of charge via the Internet at http://pubs.acs.org.

AUTHOR INFORMATION

Corresponding Authors

* grunwaldt@kit.edu (J.-D. G.)
and christoph.jacob@kit.edu (C.R.J.)

ACKNOWLEDGMENT

We thank ESRF for providing the beamtime and financial support and P. Glatzel and C. Lapras for the support during the experiments. Clariant is acknowledged for providing the parent NH_4-ZSM-5 zeolite, F. Daliran (KIT) and N.E. Nikol'skaya (FGUP "VIMS") for reference compounds, and A. Beilmann (KIT-ITCP) for the AAS measurement. M. Casapu (KIT-ITCP) is gratefully acknowledged for discussions. CRJ and AJA thank the DFG-Center for Functional Nanostructures at KIT for funding.

REFERENCES

(1) Johnson, T. *Platin. Met. Rev.* **2008**, *52*, 23.

(2) Brandenberger, S.; Kröcher, O.; Tissler, A.; Althoff, R. *Catal. Rev.* **2008**, *50*, 492.

(3) Grossale, A.; Nova, I.; Tronconi, E. *Catal. Today* **2008**, *136*, 18.

(4) Schwidder, M.; Kumar, M. S.; Klementiev, K.; Pohl, M. M.; Brückner, A.; Grünert, W. *J. Catal.* **2005**, *231*, 314.

(5) Lox, E. S. J.; Engler, B. H.; Janssen, F. J.; Garten, R. L.; Dalla Betta, R. A.; Schlatter, J. C.; Ainbinder, Z.; Manzer, L. E.; Nappa, M. J.; Parmon, V. N.; Zamaraev, K. I. In *Handbook of Heterogeneous Catalysis*; Wiley-VCH Verlag GmbH: Weinheim, Germany, 2008, p 1569.

(6) Deutschmann, O.; Grunwaldt, J.-D. *Chem. Ing. Tech.* **2013**, *85*, 595.

(7) Shelef, M. *Chem. Rev.* **1995**, *95*, 209.
(8) Long, R. Q.; Yang, R. T. *J. Catal.* **2001**, *198*, 20.
(9) Lezcano, M.; Kovalchuk, V. I.; d'Itri, J. L. *Kinet. Catal.* **2001**, *42*, 104.
(10) Apostolescu, N.; Geiger, B.; Hizbullah, K.; Jan, M. T.; Kureti, S.; Reichert, D.; Schott, F.; Weisweiler, W. *Appl. Catal. B* **2006**, *62*, 104.
(11) Bulushev, D. A.; Prechtl, P. M.; Renken, A.; Kiwi-Minsker, L. *Ind. Eng. Chem. Res.* **2007**, *46*, 4178.
(12) Metkar, P. S.; Salazar, N.; Muncrief, R.; Balakotaiah, V.; Harold, M. P. *Appl. Catal. B* **2011**, *104*, 110.
(13) Ruggeri, M. P.; Grossale, A.; Nova, I.; Tronconi, E.; Jirglova, H.; Sobalik, Z. *Catal. Today* **2012**, *184*, 107.
(14) Klukowski, D.; Balle, P.; Geiger, B.; Wagloehner, S.; Kureti, S.; Kimmerle, B.; Baiker, A.; Grunwaldt, J.-D. *Appl. Catal. B* **2009**, *93*, 185.
(15) Høj, M.; Beier, M. J.; Grunwaldt, J.-D.; Dahl, S. *Appl. Catal. B* **2009**, *93*, 166.
(16) Brüggemann, T. C.; Keil, F. J. *J. Phys. Chem. C* **2011**, *115*, 23854.
(17) Hunger, M.; Weitkamp, J. *Angew. Chem.* **2001**, *113*, 3040.
(18) Miyamoto, Y.; Katada, N.; Niwa, M. *Micropor. Mesopor. Mat.* **2000**, *40*, 271.
(19) Devadas, M.; Kröcher, O.; Elsener, M.; Wokaun, A.; Söger, N.; Pfeifer, M.; Demel, Y.; Mussmann, L. *Appl. Catal. B* **2006**, *67*, 187.
(20) Devarakonda, M.; Tonkyn, R.; Tran, D.; Lee, J.; Herling, D. *J Eng. Gas Turb. Power* **2011**, *133*, 092805.
(21) Brandenberger, S.; Kröcher, O.; Tissler, A.; Althoff, R. *Appl. Catal. B* **2010**, *95*, 348.
(22) Ott, K. C.; Clark, N. C.; Rau, J. A. *Catal. Today* **2002**, *73*, 223.
(23) Brosius, R.; Bazin, P.; Thibault-Starzyk, F.; Martens, J. A. *J. Catal.* **2005**, *234*, 191.
(24) Dubkov, K. A.; Ovanesyan, N. S.; Shteinman, A. A.; Starokon, E. V.; Panov, G. I. *J. Catal.* **2002**, *207*, 341.
(25) Maier, S. M.; Jentys, A.; Metwalli, E.; Müller-Buschbaum, P.; Lercher, J. A. *J. Phys. Chem. Lett.* **2011**, *2*, 950.
(26) Bezemer, G. L.; Remans, T. J.; van Bavel, A. P.; Dugulan, A. I. *J. Am. Chem. Soc.* **2010**, *132*, 8540.
(27) Florea, M.; Alifanti, M.; Kuncser, V.; Parvulescu, V. I. *Catal. Today* **2013**, *208*, 56.
(28) Conte, D.; Mouyane, M.; Stievano, L.; Fraisse, B.; Sougrati, M.; Olivier-Fourcade, J.; Willmann, P.; Jordy, C.; Artus, M.; Cassaignon, S.; Driezen, K.; Jumas, J.-C. *J Solid State Electrochem* **2012**, *16*, 3837.
(29) Daifuku, S. L.; Al-Afyouni, M. H.; Snyder, B. E. R.; Kneebone, J. L.; Neidig, M. L. *J. Am. Chem. Soc.* **2014**, *136*, 9132.
(30) Chandrasekaran, P.; Chiang, K. P.; Nordlund, D.; Bergmann, U.; Holland, P. L.; DeBeer, S. *Inorg. Chem.* **2013**, *52*, 6286.
(31) Lancaster, K. M.; Roemelt, M.; Ettenhuber, P.; Hu, Y.; Ribbe, M. W.; Neese, F.; Bergmann, U.; DeBeer, S. *Science* **2011**, *334*, 974.
(32) Lassalle-Kaiser, B.; Boron, T. T.; Krewald, V.; Kern, J.; Beckwith, M. A.; Delgado-Jaime, M. U.; Schroeder, H.; Alonso-Mori, R.; Nordlund, D.; Weng, T.-C.; Sokaras, D.; Neese, F.; Bergmann, U.; Yachandra, V. K.; DeBeer, S.; Pecoraro, V. L.; Yano, J. *Inorg. Chem.* **2013**, *52*, 12915.
(33) Atkins, A. J.; Bauer, M.; Jacob, C. R. *Phys. Chem. Chem. Phys.* **2013**, *15*, 8095.
(34) Westre, T. E.; Kennepohl, P.; DeWitt, J. G.; Hedman, B.; Hodgson, K. O.; Solomon, E. I. *J. Am. Chem. Soc.* **1997**, *119*, 6297.
(35) Wilke, M.; Farges, F.; Petit, P. E.; Brown, G. E.; Martin, F. *Am. Mineral.* **2001**, *86*, 714.
(36) Battiston, A. A.; Bitter, J. H.; de Groot, F. M. F.; Overweg, A. R.; Stephan, O.; van Bokhoven, J. A.; Kooyman, P. J.; van der Spek, C.; Vankó, G.; Koningsberger, D. C. *J. Catal.* **2003**, *213*, 251.
(37) Rehr, J. J.; Albers, R. C. *Rev. Mod. Phys.* **2000**, *72*, 621.
(38) Joly, Y. *Phys. Rev. B* **2001**, *63*, 125120.
(39) Delgado-Jaime, M. U.; Dible, B. R.; Chiang, K. P.; Brennessel, W. W.; Bergmann, U.; Holland, P. L.; DeBeer, S. *Inorg. Chem.* **2011**, *50*, 10709.
(40) Glatzel, P.; Sikora, M.; Smolentsev, G.; Fernández-García, M. *Catal. Today* **2009**, *145*, 294.
(41) Safonova, O. V.; Tromp, M.; van Bokhoven, J. A.; de Groot, F. M. F.; Evans, J.; Glatzel, P. *J. Phys. Chem. B* **2006**, *110*, 16162.
(42) Gallo, E.; Glatzel, P. *Adv. Mater.* **2014**, DOI: 10.1002/adma.201304994.
(43) Pollock, C. J.; DeBeer, S. *J. Am. Chem. Soc.* **2011**, *133*, 5594.
(44) Lee, N.; Petrenko, T.; Bergmann, U.; Neese, F.; DeBeer, S. *J. Am. Chem. Soc.* **2010**, *132*, 9715.
(45) Pirngruber, G. D.; Grunwaldt, J.-D.; Roy, P. K.; van Bokhoven, J. A.; Safonova, O.; Glatzel, P. *Catal. Today* **2007**, *126*, 127.
(46) Safonova, O. V.; Florea, M.; Bilde, J.; Delichere, P.; Millet, J. M. M. *J. Catal.* **2009**, *268*, 156.
(47) Gallo, E.; Bonino, F.; Swarbrick, J. C.; Petrenko, T.; Piovano, A.; Bordiga, S.; Gianolio, D.; Groppo, E.; Neese, F.; Lamberti, C.; Glatzel, P. *ChemPhysChem* **2013**, *14*, 79.
(48) Giordanino, F.; Borfecchia, E.; Lomachenko, K. A.; Lazzarini, A.; Agostini, G.; Gallo, E.; Soldatov, A. V.; Beato, P.; Bordiga, S.; Lamberti, C. *J. Phys. Chem. Lett.* **2014**, *5*, 1552.
(49) Bañares, M. A. *Catal. Today* **2005**, *100*, 71.
(50) Weckhuysen, B. M. *Phys. Chem. Chem. Phys.* **2003**, *5*, 4351.
(51) Topsøe, H. *J. Catal.* **2003**, *216*, 155.
(52) Grunwaldt, J.-D.; Clausen, B. S. *Top. Catal.* **2002**, *18*, 37.
(53) Hunger, M.; Weitkamp, J. *Angew. Chem. Int. Ed.* **2001**, *40*, 2954.
(54) Wachs, I. *Top. Catal.* **1999**, *8*, 57.
(55) Grunwaldt, J.-D.; Wandeler, R.; Baiker, A. *Catal. Rev.* **2003**, *45*, 1.
(56) Newton, M. A.; Dent, A. J.; Evans, J. *Chem. Soc. Rev.* **2002**, *31*, 83.
(57) Meunier, F. C. *Chem. Soc. Rev.* **2010**, *39*, 4602.
(58) Bare, S. R.; Ressler, T. In *Advances in Catalysis*; Bruce, C. G., Helmut, K., Eds.; Elsevier Academic Press: San Diego, USA, 2009; Vol. 52, p 339.
(59) Caravati, M.; Grunwaldt, J.-D.; Baiker, A. *Catal. Today* **2007**, *126*, 27.
(60) Rochet, A.; Moizan, V.; Pichon, C.; Diehl, F.; Berliet, A.; Briois, V. *Catal. Today* **2011**, *171*, 186.
(61) Frenkel, A. I.; Rodriguez, J. A.; Chen, J. G. *ACS Catal.* **2012**, *2*, 2269.
(62) Friebel, D.; Mbuga, F.; Rajasekaran, S.; Miller, D. J.; Ogasawara, H.; Alonso-Mori, R.; Sokaras, D.; Nordlund, D.; Weng, T.-C.; Nilsson, A. *J. Phys. Chem. C* **2014**, *118*, 7954.
(63) Merte, L. R.; Behafarid, F.; Miller, D. J.; Friebel, D.; Cho, S.; Mbuga, F.; Sokaras, D.; Alonso-Mori, R.; Weng, T. C.; Nordlund, D.; Nilsson, A.; Cuenya, B. R. *ACS Catal.* **2012**, *2*, 2371.
(64) Glatzel, P.; Weng, T.-C.; Kvashnina, K.; Swarbrick, J.; Sikora, M.; Gallo, E.; Smolentsev, N.; Mori, R. A. *J. Electron Spectrosc. Relat. Phenom.* **2013**, *188*, 17.
(65) Long, R. Q.; Yang, R. T. *Catal. Lett.* **2001**, *74*, 201.
(66) Heijboer, W. M.; Glatzel, P.; Sawant, K. R.; Lobo, R. F.; Bergmann, U.; Barrea, R. A.; Koningsberger, D. C.;

Weckhuysen, B. M.; de Groot, F. M. F. *J. Phys. Chem. B* **2004**, *108*, 10002.

(67) Grunwaldt, J.-D.; Caravati, M.; Hannemann, S.; Baiker, A. *Phys. Chem. Chem. Phys.* **2004**, *6*, 3037.

(68) Li, H. G.; Rivallan, M.; Thibault-Starzyk, F.; Travert, A.; Meunier, F. C. *Phys. Chem. Chem. Phys.* **2013**, *15*, 7321.

(69) Doronkin, D. E.; Casapu, M.; Günter, T.; Müller, O.; Frahm, R.; Grunwaldt, J.-D. *J. Phys. Chem. C* **2014**, *118*, 10204.

(70) Heijboer, W. M.; Koningsberger, D. C.; Weckhuysen, B. M.; de Groot, F. M. F. *Catal. Today* **2005**, *110*, 228.

(71) Krishna, K.; Makkee, M. *Catal. Today* **2006**, *114*, 23.

(72) Lee, H. T.; Rhee, H. K. *Catal. Lett.* **1999**, *61*, 71.

(73) Hensen, E. J. M.; Zhu, Q.; Hendrix, M. M. R. M.; Overweg, A. R.; Kooyman, P. J.; Sychev, M. V.; van Santen, R. A. *J. Catal.* **2004**, *221*, 560.

(74) Doronkin, D. E.; Piryutko, L. V.; Starokon', E. V.; Panov, G. I.; Stakheev, A. Y. *Kinet. Catal.* **2012**, *53*, 747.

(75) *Amsterdam Density Functional Program*; Vrije University Amsterdam: http://www.scm.com, accessed on 6th Aug. 2014.

(76) te Velde, G.; Bickelhaupt, F. M.; Baerends, E. J.; Guerra, C. F.; Van Gisbergen, S. J. A.; Snijders, J. G.; Ziegler, T. *J. Comput. Chem.* **2001**, *22*, 931.

(77) Becke, A. D. *Phys. Rev. A* **1988**, *38*, 3098.

(78) Perdew, J. P. *Phys. Rev. B* **1986**, *33*, 8822.

(79) Neese, F. *WIREs Comput. Mol. Sci.* **2012**, *2*, 73.

(80) Weigend, F.; Furche, F.; Ahlrichs, R. *J. Chem. Phys.* **2003**, *119*, 12753.

(81) Ryder, J. A.; Chakraborty, A. K.; Bell, A. T. *J. Phys. Chem. B* **2002**, *106*, 7059.

(82) Choi, S. H.; Wood, B. R.; Ryder, J. A.; Bell, A. T. *J. Phys. Chem. B* **2003**, *107*, 11843.

(83) Varetto, U.; 5.4.08 ed.; Swiss National Supercomputing Centre: Lugano, Switzerland, 2009.

(84) Kumar, M. S.; Schwidder, M.; Grünert, W.; Brückner, A. *J. Catal.* **2004**, *227*, 384.

(85) Ressler, T.; Timpe, O.; Neisius, T.; Find, J.; Mestl, G.; Dieterle, M.; Schlögl, R. *J. Catal.* **2000**, *191*, 75.

(86) Wang, Q.; Hanson, J. C.; Frenkel, A. I. *J. Chem. Phys.* **2008**, *129*.

(87) Fejes, P.; Kiricsi, I.; Lázár, K.; Marsi, I.; Rockenbauer, A.; Korecz, L.; Nagy, J. B.; Aiello, R.; Testa, F. *Appl. Catal. A* **2003**, *242*, 247.

(88) Kröcher, O.; Devadas, M.; Elsener, M.; Wokaun, A.; Söger, N.; Pfeifer, M.; Demel, Y.; Mussmann, L. *Appl. Catal. B* **2006**, *66*, 208.

(89) Ruggeri, M.; Nova, I.; Tronconi, E. *Top. Catal.* **2013**, *56*, 109.

(90) Cramer, S. P.; de Groot, F. M. F.; Ma, Y.; Chen, C. T.; Sette, F.; Kipke, C. A.; Eichhorn, D. M.; Chan, M. K.; Armstrong, W. H. *J. Am. Chem. Soc.* **1991**, *113*, 7937.

(91) Peng, G.; de Groot, F. M. F.; Haemaelaeinen, K.; Moore, J. A.; Wang, X.; Grush, M. M.; Hastings, J. B.; Siddons, D. P.; Armstrong, W. H. *J. Am. Chem. Soc.* **1994**, *116*, 2914.

(92) Pirngruber, G. D.; Grunwaldt, J.-D.; van Bokhoven, J. A.; Kalytta, A.; Reller, A.; Safonova, O. V.; Glatzel, P. *J. Phys. Chem. B* **2006**, *110*, 18104.

(93) Glatzel, P.; Mirone, A.; Eeckhout, S. G.; Sikora, M.; Giuli, G. *Phys. Rev. B* **2008**, *77*, 115133.

(94) Glatzel, P.; Jacquamet, L.; Bergmann, U.; de Groot, F. M. F.; Cramer, S. P. *Inorg. Chem.* **2002**, *41*, 3121.

(95) Grush, M. M.; Christou, G.; Haemaelaeinen, K.; Cramer, S. P. *J. Am. Chem. Soc.* **1995**, *117*, 5895.

(96) de Groot, F. *Coord. Chem. Rev.* **2005**, *249*, 31.

(97) Devadas, M.; Kröcher, O.; Elsener, M.; Wokaun, A.; Mitrikas, G.; Söger, N.; Pfeifer, M.; Demel, Y.; Mussmann, L. *Catal. Today* **2007**, *119*, 137.

(98) Santhosh Kumar, M.; Schwidder, M.; Grünert, W.; Bentrup, U.; Brückner, A. *J. Catal.* **2006**, *239*, 173.

(99) Maier, S. M.; Jentys, A.; Janousch, M.; van Bokhoven, J. A.; Lercher, J. A. *J. Phys. Chem. C* **2012**, *116*, 5846.

(100) Kucherov, A. V.; Montreuil, C. N.; Kucherova, T. N.; Shelef, M. *Catal. Lett.* **1998**, *56*, 173.

(101) Höfer, P. In *Electron Paramagnetic Resonance*; Brustolon, M., Giamello, E., Eds.; John Wiley & Sons, Inc.: Hoboken, New Jersey, USA, 2008, p 37.

(102) Urakawa, A.; Maeda, N.; Baiker, A. *Angew. Chem. Int. Ed.* **2008**, *47*, 9256.

(103) Nijhuis, T. A.; Tinnemans, S. J.; Visser, T.; Weckhuysen, B. M. *Chem. Eng. Sci.* **2004**, *59*, 5487.

(104) Meunier, F. C. *Catal. Today* **2010**, *155*, 164.

(105) Sirita, J.; Phanichphant, S.; Meunier, F. C. *Anal. Chem.* **2007**, *79*, 3912.

(106) Matyshak, V. A.; Krylov, O. V. *Catal. Today* **1995**, *25*, 1.

TABLE OF CONTENT GRAPHIC – ALSO FOR ABSTRACT